International Journal of Nanomedicine

Dovepress
open access to scientific and medical research

Open Access Full Text Article

ORIGINAL RESEARCH

Injectable Hydrogel Loaded with CDs and FTY720 Combined with Neural Stem Cells for the Treatment of Spinal Cord Injury

Zhiping Qi[1], Su Pan[1], Xiaoyu Yang[1], Renfeng Zhang[1], Cheng Qin[1], Hongye Yan[1], Longchuan Zhu[1], Weijian Kong[2]

[1]Department of Orthopedic Surgery, The Second Hospital of Jilin University, Changchun, 130041, People's Republic of China; [2]Department of Nuclear Medicine, The Second Hospital of Jilin University, Changchun, 130041, People's Republic of China

Correspondence: Weijian Kong; Longchuan Zhu, Email kongweijian0613@sina.com; zhulongchuan0504@163.com

Purpose: Spinal cord injury (SCI) is an incurable and disabling event that is accompanied by complex inflammation-related pathological processes, such as the production of excessive reactive oxygen species (ROS) by infiltrating inflammatory immune cells and their release into the extracellular microenvironment, resulting in extensive apoptosis of endogenous neural stem cells. In this study, we noticed the neuroregeneration-promoting effect as well as the ability of the innovative treatment method of FTY720-CDs @GelMA paired with NSCs to increase motor function recovery in a rat spinal cord injury model.

Methods: Carbon dots (CDs) and fingolimod (FTY720) were added to a hydrogel created by chemical cross-linking GelMA (FTY720-CDs@GelMA). The basic properties of FTY720-CDs@GelMA hydrogels were investigated using TEM, SEM, XPS, and FTIR. The swelling and degradation rates of FTY720-CDs@GelMA hydrogels were measured, and each group's ability to scavenge reactive oxygen species was investigated. The in vitro biocompatibility of FTY720-CDs@GelMA hydrogels was assessed using neural stem cells. The regeneration of the spinal cord and recovery of motor function in rats were studied following co-treatment of spinal cord injury using FTY720-CDs@GelMA hydrogel in combination with NSCs, utilising rats with spinal cord injuries as a model. Histological and immunofluorescence labelling were used to determine the regeneration of axons and neurons. The recovery of motor function in rats was assessed using the BBB score.

Results: The hydrogel boosted neurogenesis and axonal regeneration by eliminating excess ROS and restoring the regenerative environment. The hydrogel efficiently contained brain stem cells and demonstrated strong neuroprotective effects in vivo by lowering endogenous ROS generation and mitigating ROS-mediated oxidative stress. In a follow-up investigation, we discovered that FTY720-CDs@GelMA hydrogel could dramatically boost NSC proliferation while also promoting neuronal regeneration and synaptic formation, hence lowering cavity area.

Conclusion: Our findings suggest that the innovative treatment of FTY720-CDs@GelMA paired with NSCs can effectively improve functional recovery in SCI patients, making it a promising therapeutic alternative for SCI.

Keywords: spinal cord injury, carbon dots, FTY720, neural stem cells, hydrogel, GelMA, nerve damage repair

Introduction

Direct and rapid mechanical damage to the spinal cord causes spinal cord injury (SCI), which results in permanent motor impairments (weakness or paralysis), sensory deficiencies, and autonomic dysfunction. A cystic cavity is formed as a result of a succession of pathophysiological processes that contribute to extracellular matrix degeneration, such as inflammation, neuronal injury, and death.[1–3] The cavity hinders cellular infiltration and axon regrowth, which eventually becomes a major barrier to nerve regeneration after SCI.[4,5] Following spinal cord injury, the injured site loses a large number of endogenous neural stem cells (NSCs) as well as neurons, which is followed by an exacerbation of the secondary injury cascade, which eventually leads to the formation of a neuroglial scar around the lesion, inhibiting nerve regeneration.[6–8] Changes in the microenvironment, together

Received: 9 November 2023
Accepted: 18 April 2024
Published: 8 May 2024

with CNS neurons' lower regenerative capacity, result in a considerable decline in the self-repairing capacity of spinal cord tissues. In such cases, any treatment that focuses on a single element is unlikely to result in successful brain tissue repair.

It has been proven that concurrent therapy of cell transplantation and decrease of glial scarring following spinal cord damage can improve subsequent recovery.[9,10] Previously, biomaterials and their composite scaffold constructions were widely used in animal models to increase the proliferation and differentiation of transplanted stem cells and to minimize scarring at the transplantation site.[11,12] However, because the spinal cord injury region is frequently an irregular sac-cavity structure, typical scaffolds frequently do not suit the shape of the spinal cord injury region well, which is extremely detrimental to subsequent spinal cord injury recovery. Biomaterials and tissue engineering methods are currently potential treatments for SCI. Biomaterials with biochemical and biophysical properties similar to those of the natural spinal cord, such as electrostatically spun membranes, can be employed to aid tissue repair and regeneration.[13,14] However, bioengineered scaffolds, such as electrostatically spun silk membranes, have high mechanical qualities and distinctive morphological patterns that make them poorly populated in localised faulty areas of injury, and the most powerful therapeutic benefits are frequently limited.

Hydrogels have long been employed as scaffolds for neural tissue engineering due to their superior biocompatibility, porosity, and mechanical flexibility.[15,16] Hydrogel-based scaffold designs have been shown to have biochemical and biophysical properties similar to those of the natural extracellular matrix of the brain/spinal cord, allowing for efficient filling of irregular lesions and mimicking the physiological environment of biological tissues, thereby promoting neuronal survival and differentiation.[17] Hydrogels are widely used in the treatment of spinal cord injuries due to their unique plasticity and ability to Hydrogels are frequently employed in the treatment of spinal cord injury due to their remarkable plasticity and capacity to transport cells and growth agents. Hydrogels have a high degree of biocompatibility and degradation, as well as good modification capabilities. As a result, they may be simply adjusted to accommodate equivalent groups on their surfaces. It has been demonstrated that injectable hydrogels may successfully fill the lesion cavity and adhere to the shape of the defect, blending smoothly with the host tissue.[18] Another benefit of injectable hydrogels is that they can be injected directly into the target area or tissue using minimally invasive procedures, hence preventing secondary damage.[19,20] Another advantage of injectable hydrogels is that they can be injected directly into the target area or tissue using minimally invasive procedures, hence preventing secondary harm. Based on these features, the current study decided to use GelMA, an injectable hydrogel, as a carrier to fill the hydrogel in situ in the wounded area, providing greater nutritional and supporting protection.

One of the most significant alterations in spinal cord injury is an increase in reactive oxygen species (ROS) localized to the damage.[21,22] According to growing data, dramatically higher levels of reactive oxygen species (ROS) within the injured spinal cord play an important role in the secondary injury cascade response.[23] Scavenging ROS is thus an effective method to reduce subsequent harm following acute spinal cord injury.[24–26] Carbon dots (CDs) are nanoscale particles that have received a lot of attention in the biological arena. Carbon dots, due to their biocompatibility and hydroxyl and carboxyl structures on their surfaces, can considerably suppress the production of reactive oxygen species (ROS) in the wounded area and reduce local inflammation, hence aiding injury repair.[27] Furthermore, carbon dots can be changed by various synthetic procedures, and other chemical groups can be added to their surface to enhance their biological capabilities. Selenium-doped carbon dots (Se-CDs) have been discovered to be a type of modified carbon dots generated by hydrothermal treatment of L-selenocysteine. After oxidative damage, it shows a clear protective impact on astrocytes and PC12 cells. Furthermore, Se-CDs outperformed carbon dots alone in terms of anti-inflammatory and anti-apoptotic activity.[28,29]

As previously stated, one of the key changes that occurs after spinal cord injury is the loss of endogenous neural stem cells (NSCs) as well as neurons.[30,31] As a result, finding techniques to stimulate neuronal to neuronal development of endogenous neural stem cells at the damage site is critical. Fingolimod (FTY720) is a type of drug used to treat multiple sclerosis, and existing studies have shown that FTY720 can reduce neural stem cell differentiation to astrocytes and promote neural stem cell proliferation to a certain extent, which has good neuroprotective effects and a wide range of prospects for application in spinal cord injury.[32–34] As a result, in the current study, we decided to include FTY720, a drug co-loaded with NSCs in a hydrogel, to synergize the effect and jointly promote the proliferation and differentiation of neural stem cells in the local area of spinal cord injury, as well as to reduce the formation of astrocytes, which reduces scarring of the injured area.

In this study, a GelMA hydrogel loaded with FTY720 CDs (FTY720-CDs@GelMA) was innovatively created so that it coupled with NSCs to fill the capsular cavity of spinal cord injuries via in situ injection to promote spinal cord healing (Schematic 1). The resultant hydrogel has good biocompatibility and ROS scavenging capabilities, and it has been shown in vitro to have considerable protective effects on astrocytes and NSCs. Furthermore, FTY720-CDs@GelMA hydrogel implantation boosted neuronal differentiation of transplanted NSCs, decreased glial scar formation, and aided axonal regeneration and neural circuit repair. The results demonstrated that combining FTY720-CDs@GelMA hydrogel with NSCs greatly improved motor function recovery after spinal cord damage in rats, suggesting a new strategy for the holistic treatment of spinal cord injury.

Materials and Methods

Preparation and Characterization of Carbon Dots

Water-soluble Se-CDs were created using a previously disclosed method.[27] In 10 mL of deionized water, 200 mg of L-selenocysteine was dissolved. When the reaction temperature reached 60 °C, the bright yellow selenocysteine solution changed to an orange-brown colour after the pH was adjusted to 9. The solution was then heated for 24 hours at 60 degrees Celsius. After centrifuging the brown solution at 10,000 rpm, the supernatant was collected and dialyzed. The freeze-dried Se-CDs solution produced a brown powder. Distillation was employed to extract the solvent, which was then dried before being used in further testing. The properties and characterization of the resultant Se-CDs after successful preparation were investigated using transmission electron microscopy (TEM), Fourier transform infrared spectroscopy (FTIR), and X-ray photoelectron spectroscopy (XPS). The zeta potential of Se-CQDs was determined with a Zetasizer Pro (Malvern Panalytical Ltd, Worcestershire, UK).

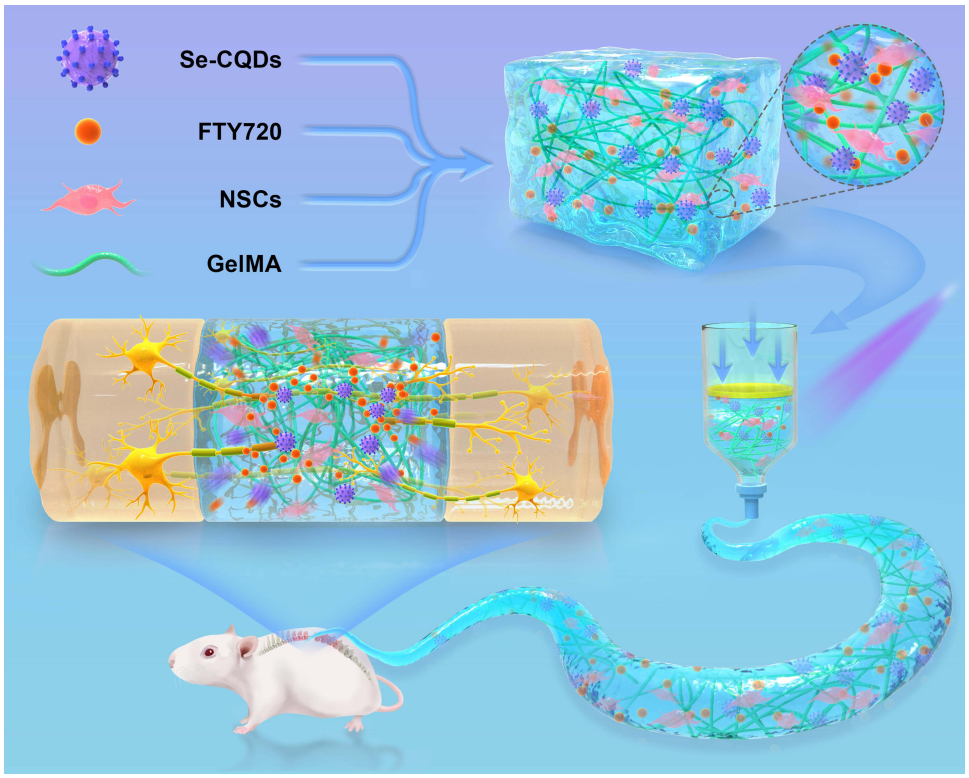

Schematic 1 This paper's schematic diagram. FTY720-CDs@GelMA hydrogel was prepared, filled with NSCs, and implanted into a rat spinal cord total transection damage model. This combination therapy enhances nerve regeneration and functional recovery by boosting the proliferation and differentiation of endogenous neural stem cells into neurons, while also drastically reducing gliogenesis at the lesion site.

Preparation and Characterization of GelMA Hydrogels Loaded with Carbon Dots as Well as FTY720

First, 10 μg mL^{-1} of Se-CDs and 15 μg mL^{-1} of FTY720 were dissolved in phosphate buffer solution (PBS, pH=7.4), respectively. GelMA was dissolved in PBS with Se-CDs (concentration: 10 μg mL^{-1}) and FTY720 (15 μg mL^{-1}). GelMA hydrogels containing CDs and FTY720 were then cured for 30 seconds under UV irradiation to generate a GelMA hydrogel. The same approach was used to create CDs@GelMA hydrogels, FTY720@GelMA hydrogels, and GelMA hydrogels. Following UV sterilization, all hydrogels were employed in following tests. Scanning electron microscopy was used to analyze the hydrogels' characteristics. SEM was used to examine the morphology of the hydrogels. Following that, the porosity, swelling rate, and degradation rate of the four created hydrogels were examined in order to assess whether the four hydrogels are biocompatible.

Cumulative Release Estimation of Se-CDs from Hydrogels

Add 7 mL of CDs@GelMA hydrogel to a centrifuge tube with 21 mL of phosphate. The assembly was shaken at 37°C and 150 RPM. At predetermined time intervals, 3 mL aliquots were withdrawn and replenished with PBS. Having adjusted to 10 mL, the samples were injected. The samples' Se-CDs content was evaluated using an external standard, an Agilent 5110 inductively coupled plasma mass spectrometer.

The total number of Se-CDs released in this investigation is designated by Q, the liquid concentration in the ith replacement sample is Ci, and the prior (i-1) replacement sample is C_{i-1}. V_i is the replacement receiving solution volume, and V is the 21-mL released medium volume. "n" reflects the number of times the receiving solution was replenished and "m" represents the hydrogel's Se-CDs mass.

$$Q(\%) = \frac{C_i \times V + \sum_{i-1}^{n-1} C_{i-1} \times V_i}{m} \times 100\%$$

Determination of Biocompatibility of Hydrogels Loaded with Carbon Dots

Cell live-dead staining, in vivo hydrogel degradation, and visceral toxicity assays were used to confirm the biocompatibility of the hydrogels in the GelMA, CDs@GelMA, FTY720@GelMA, and FTY720-CDs@GelMA groups.

First, NSCs were seeded at 1×10^4 mL^{-1} on the surface of the hydrogels of the four groups mentioned above, and the cells were collected after 24 hours of cell culture and stained with a cell live-dead staining kit (Sigma-Aldrich). Fluorescence microscopy was used to study the cell development of NSCs injected in hydrogels.

In the in vivo hydrogel degradation test, GelMA, CDs@GelMA, FTY720@GelMA, and FTY720-CDs@GelMA hydrogels were put subcutaneously on the backs of different SD rats. The rats were killed at regular intervals, and images were taken to document the weight of the hydrogels in each group.

Finally, to further evaluate the biocompatibility of CDs and whether toxic aggregation or inflammation would occur after the introduction of CDs as nanoparticles, four hydrogels with different concentrations were implanted subcutaneously into SD rats, who were executed on the seventh day after the implantation, and paraffin sections of the rats' visceral organs were taken and subjected to HE staining, in order to observe the histomorphology of the organs.

Reactive Oxygen Scavenging Assessment

The efficacy of FTY720-CDs@GelMA to scavenge reactive oxygen species was assessed using three methods: DPPH, ROS, and DHE. The experimental groups were the same as in the section on biocompatibility validation.

A DPPH kit (BC4750, Solarbio, China) was used to test the ability of FTY720-CDs@GelMA hydrogel to scavenge free radicals. 100 μL of hydrogel was mixed with 100 μL of solution and incubated in the dark at room temperature for 30 minutes before measuring absorbance (At) at 517 nm. As a blank control (Ac), PBS was added. Scavenging rate of DPPH=(Ac-AT)/Ac×100%.

Using a reactive oxygen species detection kit (Beyotime, China), the effect of four sets of hydrogels on the elimination of cellular reactive oxygen species was examined. NSCs were inoculated on hydrogels at a density of 5×10^4 mL^{-1}, the medium was removed after 3 days of incubation, the cells were stimulated with 100 μM H_2O_2 for 30

minutes and then washed away with PBS to remove H_2O_2, and DCFH-DA was incubated for 20 minutes and then washed away with PBS to remove unbound DCFH-DA, and fluorescent intensity of each group of hydrogels was measured using fluorescence microscopy.

The DHE kit (Bestbio, China) was used to test the in vivo reactive oxygen species scavenging effect of FTY720-CDs @GelMA. After 24 hours, the hydrogels were implanted into the leg muscles of rats, and the muscle tissues were collected and freeze sectioned. After incubating the DHE probes at room temperature for 1 hour, the unbound DHE was washed away with PBS, and the in vivo tissue reactive oxygenation was evaluated using fluorescence microscopy.

Isolation, Culture and Characterization of NSCs

The Animal Protection and Use Ethics Committee of Jilin University (2019032) authorized all animal experimental protocols. At 13–14 days of gestation, neural stem cells were extracted from the hippocampus region of the brain of fetal rats. Cells were grown at a density of 2×10^4 mL in T25 culture flasks. DMEM/F12 (Gibco, USA), 2% B27 neural supplement (Gibco, USA), 20 ng mL^{-1} epidermal growth factor (EGF; Invitgen, USA), 20 ng mL^{-1} basic fibroblast growth factor (bFGF, Sigma), and 100 ng mL^{-1} penicillin-streptomycin (Gibco Invitgen) were used in the proliferation medium. The culture medium was replaced every 2 days, and neural stem cells were passaged and cultivated every 4 days; the second through fifth generations of neural stem cells were employed for following cell tests.

The NSCs were then transferred to 24-well plates prepped with 10% polylysine and cultured for 12 hours in a cell culture incubator before the media was removed and 4% paraformaldehyde fixative was added to each well and fixed at room temperature for 30 minutes. Following the removal of the paraformaldehyde, the wells were rinsed three times with PBS buffer to eliminate any remaining paraformaldehyde, and then 10% goat serum was added to each well and closed for 1 hour at room temperature. For 1 hour, the wells were closed at room temperature. After aspirating the excess serum, the immunofluorescent primary antibody (Nestin, Abcam) produced with antibody diluent was applied to each well, and the wells were incubated at 37°C for 2 hours. PBS buffer containing 5% goat serum and 1‰ Triton-X 100 was used as an antibody diluent, and the unbound Nestin primary antibody was aspirated away from the wells using PBS buffer, and the immunofluorescent primary antibody was introduced to the wells with PBS buffer. The unbound Nestin primary antibody was washed from each well with PBS buffer before adding the prepared FITC secondary antibody (Alexa-Fluor 488, Invitgen) and incubating for 2 hours at room temperature. The unbound primary antibody was rinsed off with PBS, and the cell nuclei were stained with DAPI dropwise in each well, with the findings viewed using a laser confocal microscope.

Proliferation and Differentiation of NSCs in Hydrogels

The CCK-8 technique was used to assess the growth of NSCs in GelMA, CDs@GelMA, FTY720@GelMA, and FTY720-CDs@GelMA hydrogels. NSCs were injected in 24-well plates at a concentration of 3.0×10^4 mL^{-1} in the four hydrogel groups mentioned above. On days 1, 4, and 7, the CCK-8 assay was performed by adding CCK-8 solution to each well and incubating at 37°C for 2 hours. An enzyme meter was used to detect the absorbance at 450 nm.

The differentiation of neural stem cells in different hydrogels was detected using immunofluorescence labeling and real-time quantitative polymerase chain reaction (qRT-PCR). As previously reported, the NSCs differentiation experimental groupings were divided into four groups: the GelMA group, the CDs@GelMA group, the FTY720@GelMA group, and the FTY720-CDs@GelMA group. Different groups of neural stem cells were cultivated for 7 days and labeled with Tuj-1 antibody (1:500, Abcam, USA) to observe neural stem cell differentiation and synaptic growth. To detect the differentiation of neural stem cells to astrocytes, separate groups of hydrogel neural stem cells were labeled with GFAP antibody (1:500, Abcam, USA). The immunofluorescence staining approach was the same as that used to identify neural stem cells.

qRT-PCR Analysis

Total RNA was extracted using Trizol reagent (Invitrogen, USA) according to the manufacturer's plan after 7 days of differentiation culture under varied settings for further quantitative study of NSC differentiation under different conditions. A Nanodrop spectrophotometer (Tecan, Switzerland) was used to assess total RNA concentration and purity. Using the PrimeScript kit (TAKARA, CHINA), the RNA samples were reverse transcribed into cDNA for qPCR. Table 1 displays the

Table 1 Primer Sequences

Gene	Forward Primer	Reverse Primer
Tuj-1	GATCGGAGCCAAGTTCTG	GTCCATCGTCCCAGGTTC
GFAP	GCAGACCTTCTCCAACCTG	ACTCCTTAATGACCTCTCCATC
GAPDH	TCGCCAGCCGAGCCA	CCTTGACGCTGCCATGCAAT

primer sequences for the target gene. The qPCR program began with a 10-minute denaturation at 95°C, followed by 40 cycles of 95°C for 30 seconds, 58°C for 1 minute, and 72°C for 1 minute. GAPDH as an internal control gene.

Construction of an Animal Model of Spinal Cord Injury

All procedures involving rats adhered to the guidelines provided by the Institutional Animal Care and Use Committee of Jilin University (Changchun, P. R. China, KT202203069). Adult female SD rats weighing 200–250 g were purchased from Jilin University's Experimental Animal Center. The experimental animals were kept in a constant temperature chamber with a temperature of (23±2°C) and a photoperiod of 12/12h, and they had free access to water and food until they were used.

All rats were separated into five groups: the GelMA group, the CDs@GelMA group, the FTY720@GelMA group, the FTY720-CDs@GelMA group, and the FTY720-CDs+NSCs group. Six rats in each group, 30 in total.

To create a rat spinal cord total excision damage model, the following procedure was employed. The rats were sedated with sodium pentobarbital at a dose of 30 mg/kg body weight. To reveal the thoracic spinal cord segments, a T9 laminectomy was performed. The spinal cord tissue was removed with ophthalmic scissors, gauze was used to stop the bleeding, and saline was rinsed before being implanted into the GelMA group, the CDs@GelMA group, the FTY720@GelMA group, the FTY720-CDs@GelMA group, and the FTY720-CDs+NSCs group, according to experimental groupings. The soft tissues were sutured and the skin was closed layer by layer. To prevent bladder pee accumulation, postoperative therapy included aided voiding three times per day. During infection prevention, penicillin 100,000 units/kg each rat was administered intramuscularly daily during the first three postoperative days.

BBB Score

The BBB score was used in this investigation to determine recovery of motor function following spinal cord damage in all groups of rats, who were assessed weekly for 8 weeks. Two independent reviewers who were ignorant of the animals' treatments rated all rats weekly over a 4-minute period.

Histologic Staining and Immunofluorescent Staining

After 8 weeks, the rats were killed, and the spinal cord tissues were fixed with 4% paraformaldehyde for 24 hours and dehydrated with 30% sucrose for 24 hours. The treated spinal cord tissues were cryosectioned at 20 μm thickness, stained with hematoxylin and eosin, and examined under a light microscope. The immunofluorescence staining procedure was as follows. Sections were fixed with antigen repair solution and treated for 30 minutes with 5% goat serum. Tuj-1 (1:500, ab7751, Abcam) and NF200 (1:200, ab3966, Abcam) immunofluorescent primary antibodies were put on slides and incubated at 4°C for 24 hours before being washed with PBS. After incubating in the dark at room temperature for 40 minutes, immunofluorescent secondary antibodies (Alexa Fluor 488, 1:400; Alexa Fluor 594, 1:800; Invitgen) and free antibodies were removed by washing with PBS. Finally, DAPI-labeled nuclei were added to the slices, which were then sealed with glycerol and examined using a fluorescence microscope.

Statistical Analysis

All quantitative data were analyzed with GraphPad Prism 5.0 software (GraphPad software, USA) and expressed as mean ± standard deviation. One-way analysis of variance (ANOVA) was used for more than two variables, and *t*-test was used for two variables. $p < 0.05$ was considered statistically significant.

Results

Preparation and Characterization of CDs

Scanning electron microscopy was used to evaluate the properties of the prepared Se-CDs. Figure 1A shows that the prepared Se-CDs have a nanoscale structure. The scanning electron microscopy results (Figure 1A) showed that Se-CDs had been successfully synthesised. The Se-CDs were spherical in form, with an average diameter of around 19 nm. The relatively tiny particle size of the manufactured carbon dots could be explained to shrinkage of the shell layer during sample preparation and drying. The zeta potential of prepared Se-CQDs was −16.2 ± 0.34. The molecular structure of the Se-CDs was further characterised using FTIR infrared spectroscopy. As illustrated in Figure 1B and C), the FTIR spectra revealed that Se-CDs had a different chemical structure than the precursor molecule L-selenocysteine, confirming the chemical conversion of L-selenocysteine to Se-CDs. The XPS spectra revealed that the Se-CDs were mostly composed of carbon, nitrogen, selenium, and oxygen, agreeing with the normal peaks of C 1s, N 1s, O 1s, and Se 3d. The effective synthesis of Se-CDs has been proven.

Characterization of Hydrogels and Free Radical Scavenging Assay

CDs and FTY720 were added to GelMA solution, and UV radiation curing technology was used to successfully prepare CDs@GelMA, FTY720@GelMA, and FTY720-CDs@GelMA hydrogels (Figure 2A), with the external image demonstrating

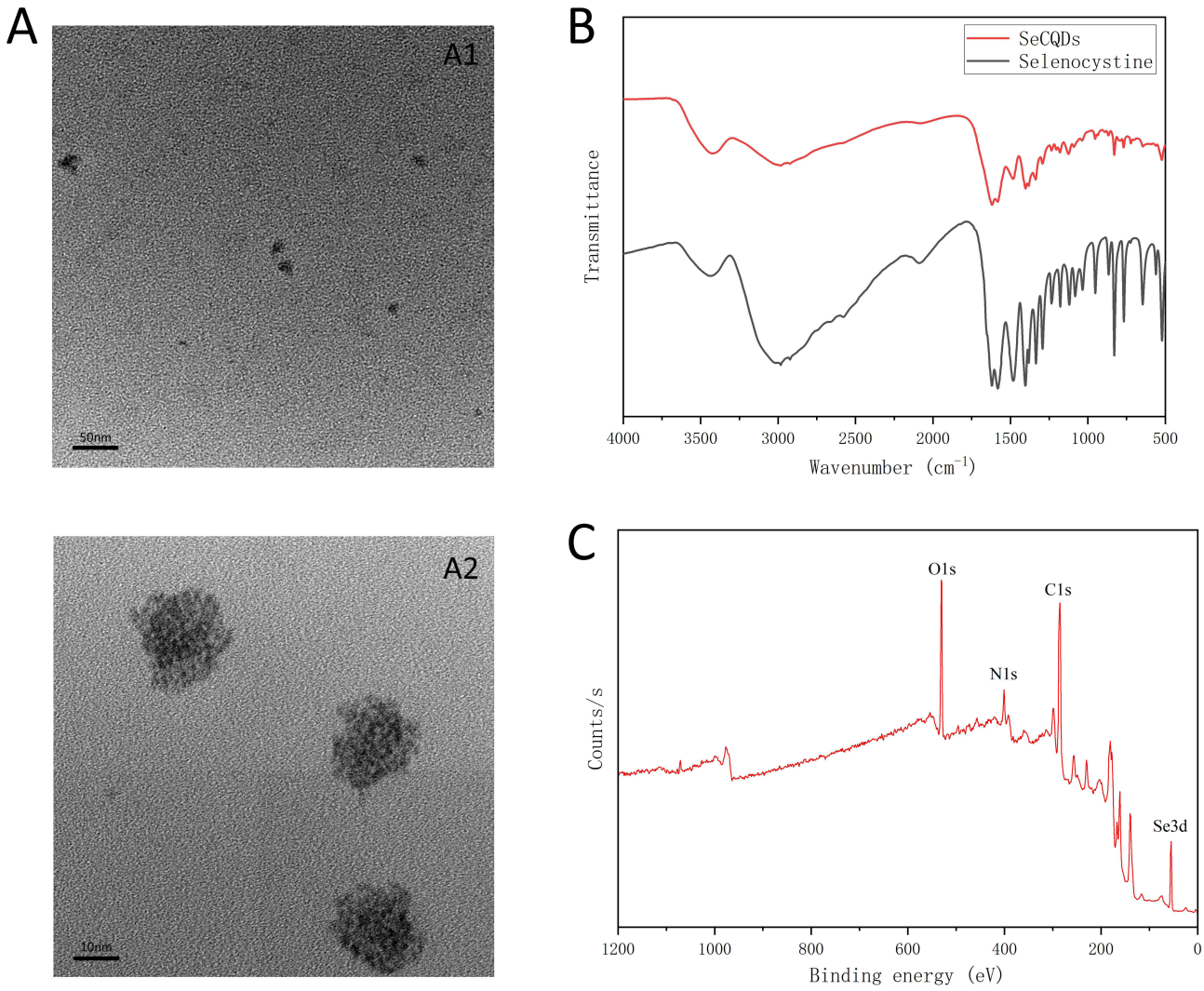

Figure 1 Characterization of the prepared carbon dots. (**A**) TEM image of the CDs. A1: low magnification, scale bar:50 nm; A2: high magnification, scale bar:10 nm. (**B**) FTIR results of the prepared carbon dots. (**C**) XPS spectra of the prepared carbon dots.

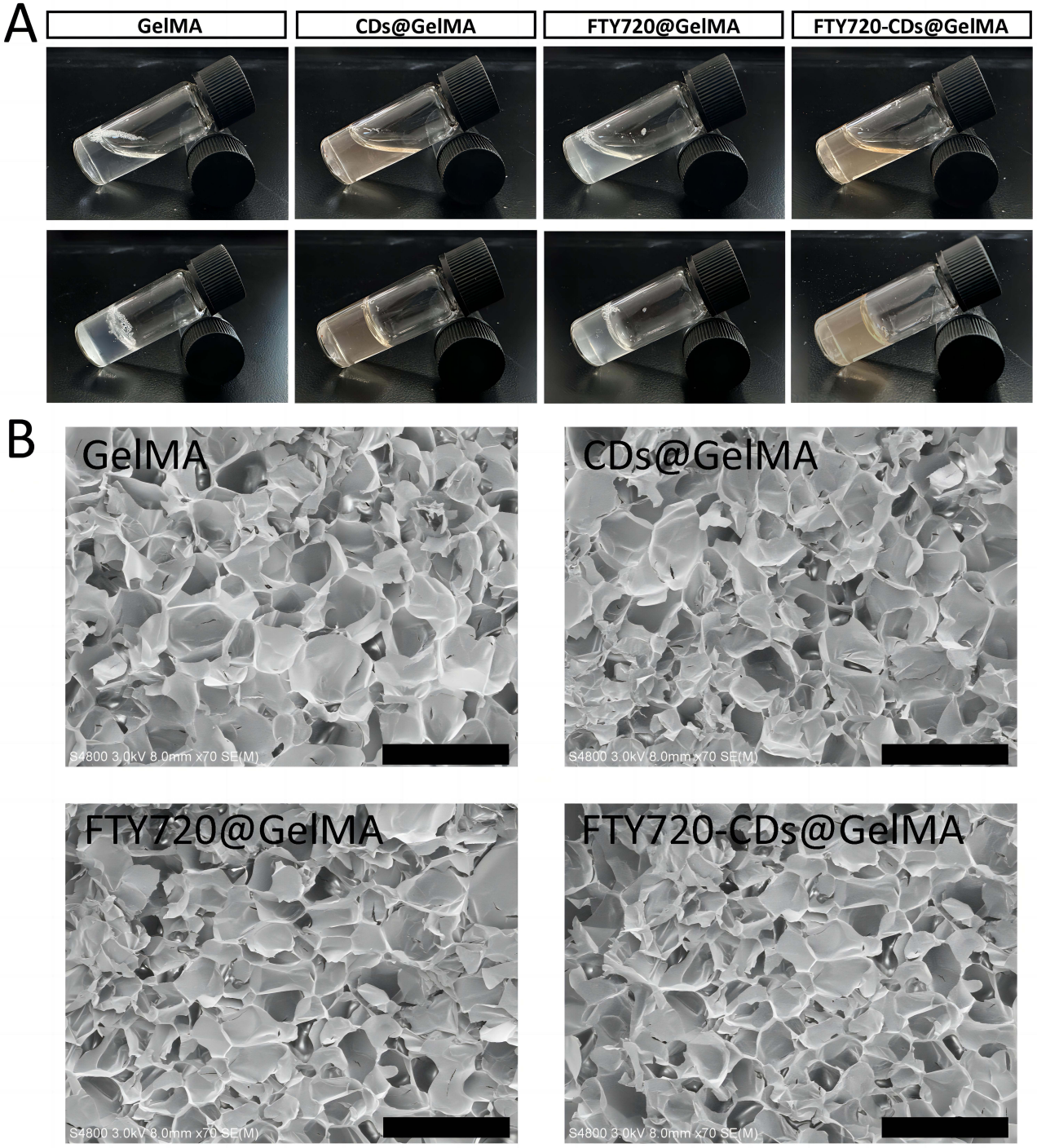

Figure 2 Characterization of different groups of hydrogels prepared. (**A**) External image of different groups of hydrogels formed into gel. (**B**) Pore structure of different hydrogels under scanning electron microscope. Scale bar: 500 μm.

that the hydrogels could be converted from a liquid to a solid state at room temperature. SEM analysis revealed that the various groups of hydrogels prepared had suitable pores, and these loose pore-like structures of the hydrogels were favorable for cell and drug adhesion, allowing for better nutritional support after in situ transplantation in the region of the spinal cord injury (Figures 2B and 3A).

SEM was used to examine the gel-forming condition and microscopic pore size of various groups of hydrogels (Figure 2). The prepared hydrogels of different groups had suitable pores, as shown in Figure 2B, and these loose pore-like structures of

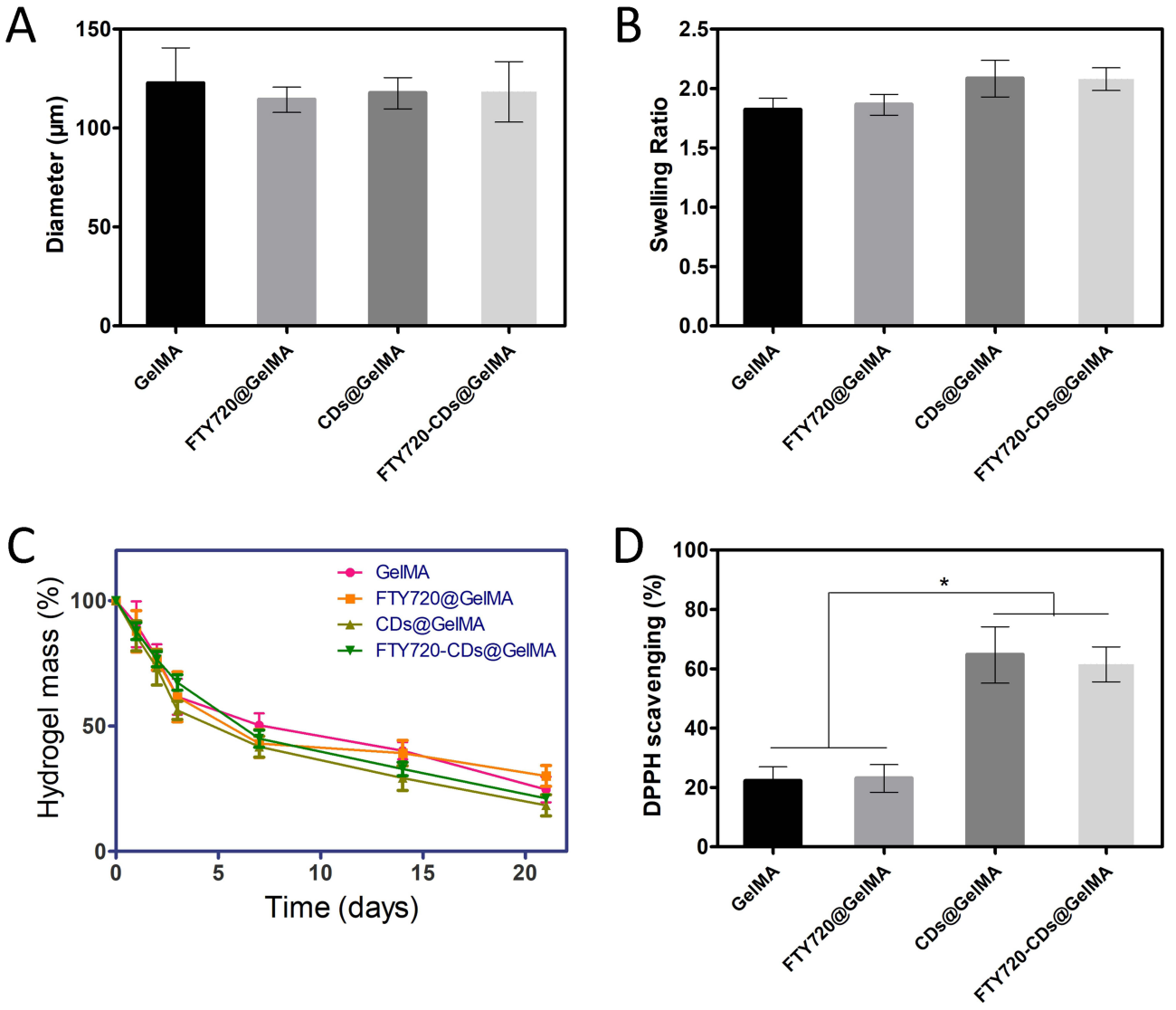

Figure 3 Characterization and reactive oxygen scavenging capacity of different groups of hydrogels. (**A**) Diameter size of different hydrogel pores. (**B**) Dissolution rate of different groups of hydrogels. (**C**) Degradation time curve of different groups of hydrogels. (**D**) Free radical scavenging capacity of different groups of hydrogels. *P<0.05.

the hydrogels were favorable for the adhesion of cells as well as drugs, so they could play a better role in nutritional support after in situ transplantation in the region of spinal cord injury. The swelling rates of various hydrogels revealed that the three hydrogels had similar swelling rates ranging from 150% to 250%, with the CDs@GelMA hydrogel having a slightly higher swelling rate of 210% (Figure 3B). The hydrogels' adequate swelling capacity meant that they could completely fill the voids after implantation without shifting or dislocating. In Figure 3B, each group of hydrogels demonstrated a good swelling rate, indicating that each group of hydrogels had strong swelling capacity and could successfully fill the hollow area after spinal cord injury with a better filling effect. Following degradation rate measurements of the hydrogels in each group (Figure 3C), we confirmed that the hydrogel's in vitro degradation time is approximately 21 days, aligning with the natural healing process of spinal cord injuries. This indicates that the hydrogel will not degrade rapidly after implantation. The hydrogel's degradation time matches the endogenous repair time of spinal cord injuries, allowing it to provide slow-release components at the site of injury, enhancing its effectiveness.

Following spinal cord damage, a high number of nerve cells in the affected area die, and dendrites and axons are demyelinated. Furthermore, subsequent ischemia/reperfusion injury causes a high amount of ROS to be released in the injured location, and inflammatory cells in the body begin to move to the injured area in response to ROS stimulation,

resulting in a localized inflammatory response. The buildup of ROS and inflammatory cells worsens the spinal cord damage. Later in the healing process, neural stem cells develop into astrocytes and generate a huge number of glial scars to fill the wounded area, further obstructing the connection between the two ends of the injury. In view of the numerous adverse conditions stated above, relying solely on endogenous neural stem cells to repair motor and sensory functions following spinal cord injury is insufficient. To investigate the ROS scavenging effects of several groups of hydrogels, we assessed the DPPH, ROS, and DHE scavenging effects at three levels: material, in vitro cellular, and in vivo tissue. The absorbance of the solution following the addition of hydrogels to the DPPH solution was measured to assess the scavenging impact of different hydrogels on free radicals. The CDs@GelMA hydrogel could scavenge more than 70% of the free radicals in the solution, while FTY720-CDs@GelMA could scavenge around 65%; the scavenging impact of both groups was substantially higher than that of the FTY720@GelMA and GelMA groups (Figure 3D).

Release of Se-CDs from the Hydrogels

Investigation of the release kinetics of Se-CDs from various hydrogel matrices is warranted due to their critical function in facilitating neurite-to-neurite differentiation in neural stem cells and scavenging reactive oxygen species upon release from hydrogels. The findings are illustrated in Figure S1, which demonstrates that Se-CDs experienced a phase of accelerated release within the initial three days, accumulating at a rate of 43.1% by day three. After three days, the discharge of Se-CDs slowed and on day seven, it approached equilibrium. The cumulative release rate on day fourteen was 76.6% in the hydrogel group, indicating that Se-CDs were completely released. The prolonged bioactivity of Se-CDs was not only ensured by this release, but also their capacity to scavenge reactive oxygen species and stimulate neuronal differentiation into neural stem cells was validated.

Determination of Biocompatibility of Different Groups of Hydrogels

CCK8 and cell live-dead staining were used in this work to determine the cytocompatibility of the hydrogels in each experimental group. Figure 4 shows that the FTY720-CDs@GelMA hydrogel group had the maximum number of living cells as well as the best cellular activity, showing that the FTY720-CDs@GelMA hydrogel may provide a suitable survival environment for NSCs. This prepared the path for the next phase of SCI co-treatment with NSCs.

Subsequently, we established the visceral toxicity of FTY720-CDs@GelMA hydrogel by HE staining. As demonstrated in Figure 5, no deposition of CDs was shown in the organs of rats in all groups within 7 days after implantation, however, no evident inflammatory reaction or pathological alterations were seen in the organs of all groups. This implies that the

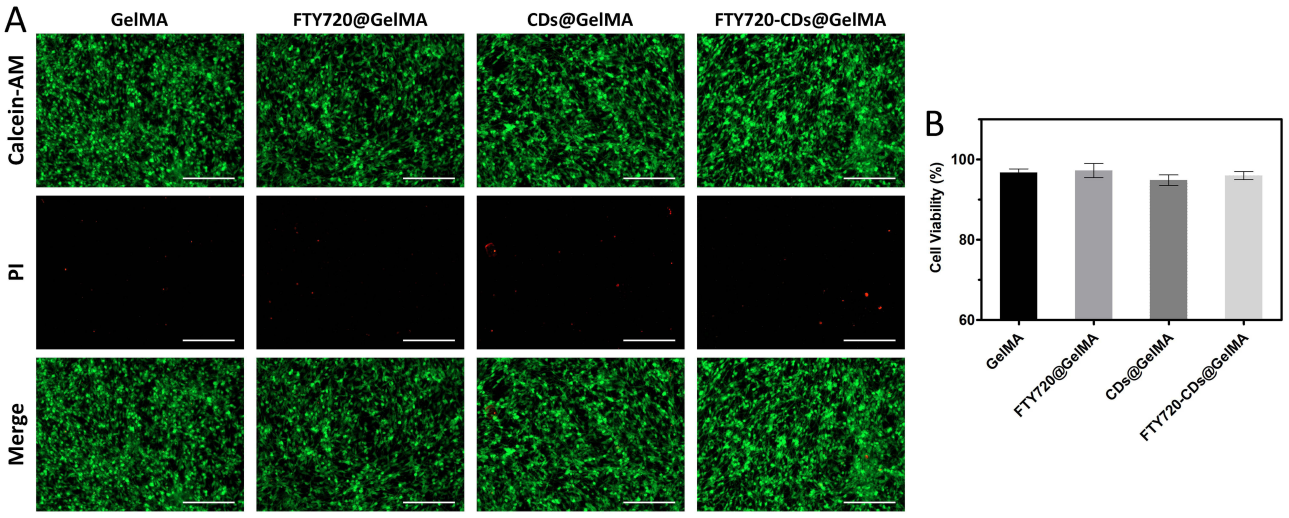

Figure 4 Live-dead staining images of NSCs after culture in different groups of hydrogels. (**A**) Live-dead staining; green: live cells; red: dead cells. Scale bar: 200 μm. (**B**) survival of neural stem cells in different groups of hydrogels.

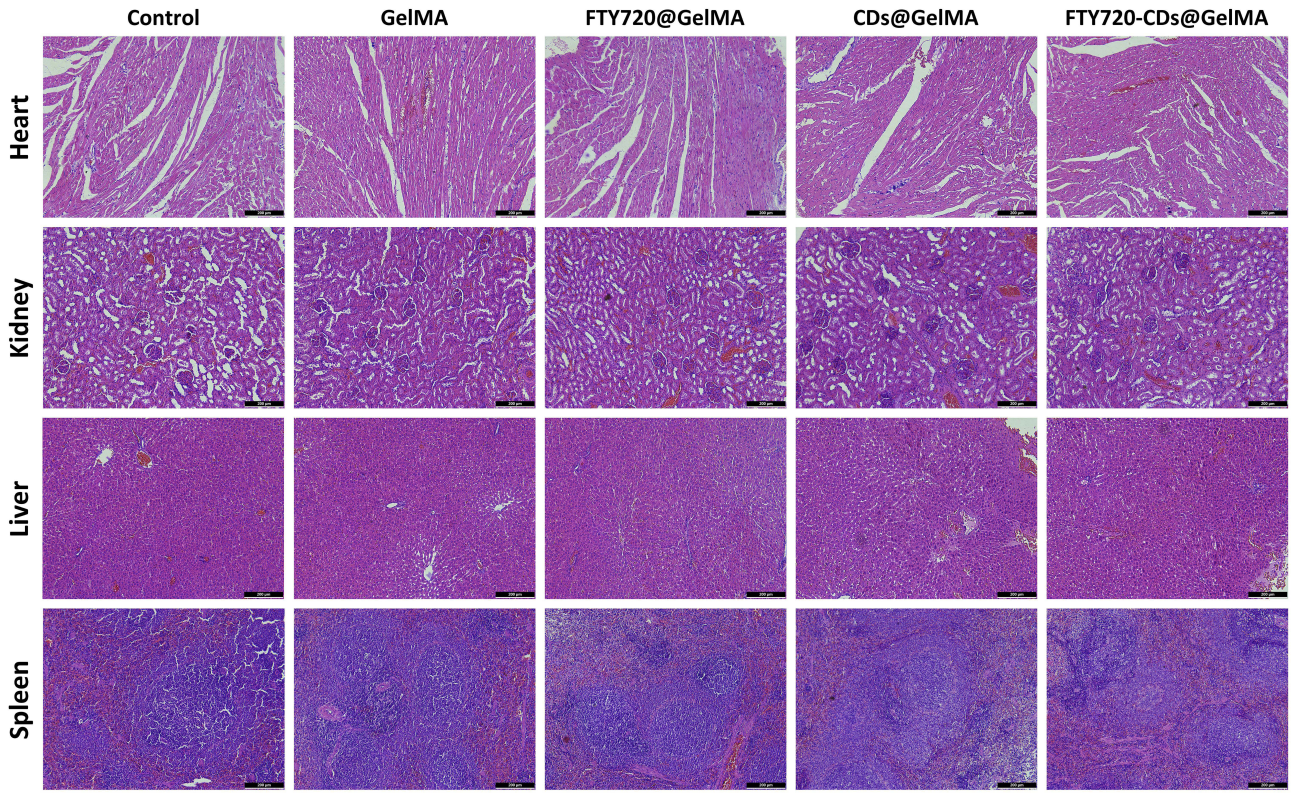

Figure 5 Histological morphology of major organs (heart, kidney, liver and spleen) after implantation of different types of hydrogels. Shown in the figure are Control: blank control group; GelMA: injectable hydrogel group alone; FTY720@GelMA: injectable hydrogel group loaded with FTY720; CDs@GelMA: injectable hydrogel group loaded with CDs; FTY720-CDs@GelMA: injectable hydrogel group loaded with FTY720 and CDs. FTY720-CDs@GelMA: injectable hydrogel set loaded with FTY720 and CDs. Scale bar: 200μm.

introduction of CDs did not produce toxicity buildup after implantation of the four groups of hydrogels, confirming that the four groups of hydrogels have good biocompatibility and can be employed in following in vivo research.

Scavenging Effect of Reactive Oxygen Species in Different Groups of Hydrogels

We then used a ROS kit to confirm the protective impact of FTY720-CDs@GelMA on cells in order to investigate the ROS scavenging effect of different groups of hydrogels (Figure 6A). The results showed that the number of ROS-positive cells was significantly lower in the CDs@GelMA group compared to the FTY720@GelMA and GelMA groups, and the number of ROS-positive cells was even lower in the FTY720-CDs@GelMA group, with a statistically significant difference when compared to the CDs@GelMA group (Figure 6C). This beneficial scavenging effect may be related to CDs' extraordinary free radical scavenging capabilities. Using the DHE kit, the ROS scavenging function of FTY720-CDs@GelMA hydrogels in in vivo tissues was investigated (Figure 6B). DHE expression was up-regulated the greatest in the control and GelMA groups and the least in the FTY720@GelMA group, according to immunofluorescence staining. However, DHE expression was further down-regulated in the CDs@GelMA and FTY720-CDs@GelMA groups, with statistically significant differences compared to the GelMA and FTY720@GelMA groups (Figure 6D). The preceding experimental results showed that the CDs@GelMA and FTY720-CDs @GelMA groups had better ROS scavenging effects, with the FTY720-CDs@GelMA group having the best scavenging effect.

Proliferation and Differentiation of NSCs in Different Groups of Hydrogels

The fetal rat cerebral cortex cells were identified using immunofluorescence labeling. The results revealed that all removed cells expressed positive Nestin, indicating that the cells were neural stem cells. Nestin expression was persistent in cells inoculated in FTY720-CDs@GelMA hydrogel (Figure 7A). Following that, we transplanted the isolated NSCs into different groups of hydrogels for growth and performed CCK8 tests at 1d, 4d, and 7d, with the results given in Figure 7B, indicating

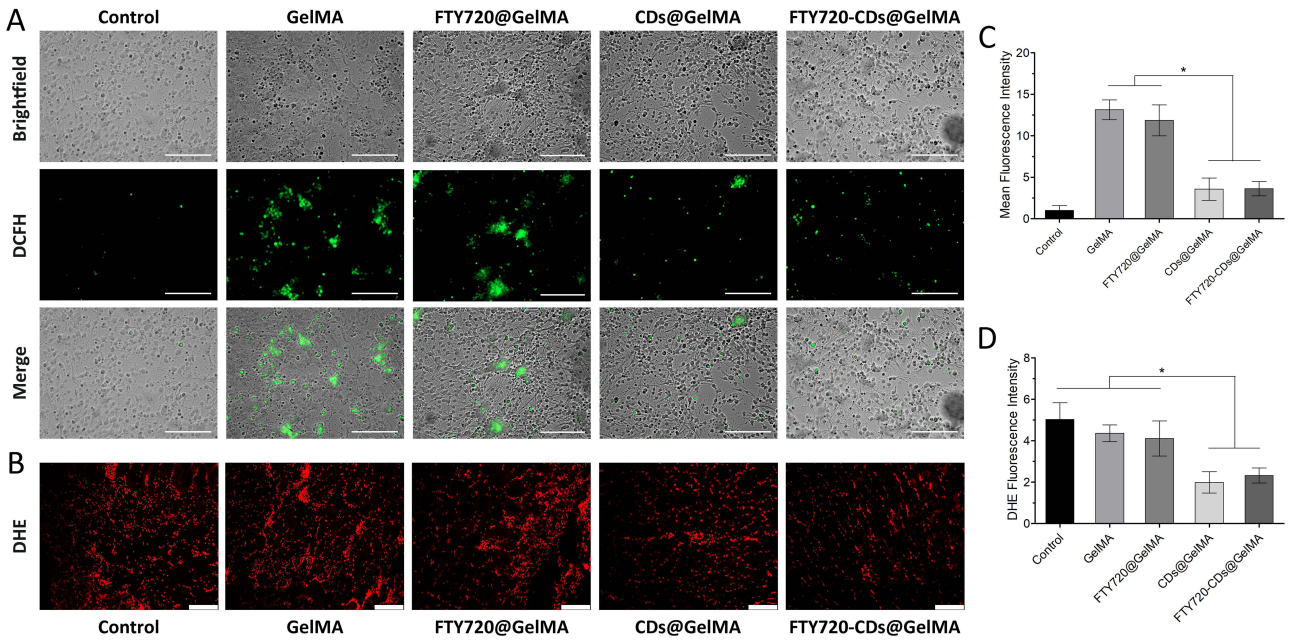

Figure 6 Scavenging of reactive oxygen species by different groups of hydrogels. (**A**) DCFH images of different groups of hydrogels. Scale bar: 200 μm. (**B**) DHE images of different groups of hydrogels. Scale bar: 200 μm. (**C**) average fluorescence intensity of hydrogels of different groups. (**D**) DHE fluorescence intensity of different groups. *Indicates P<0.05.

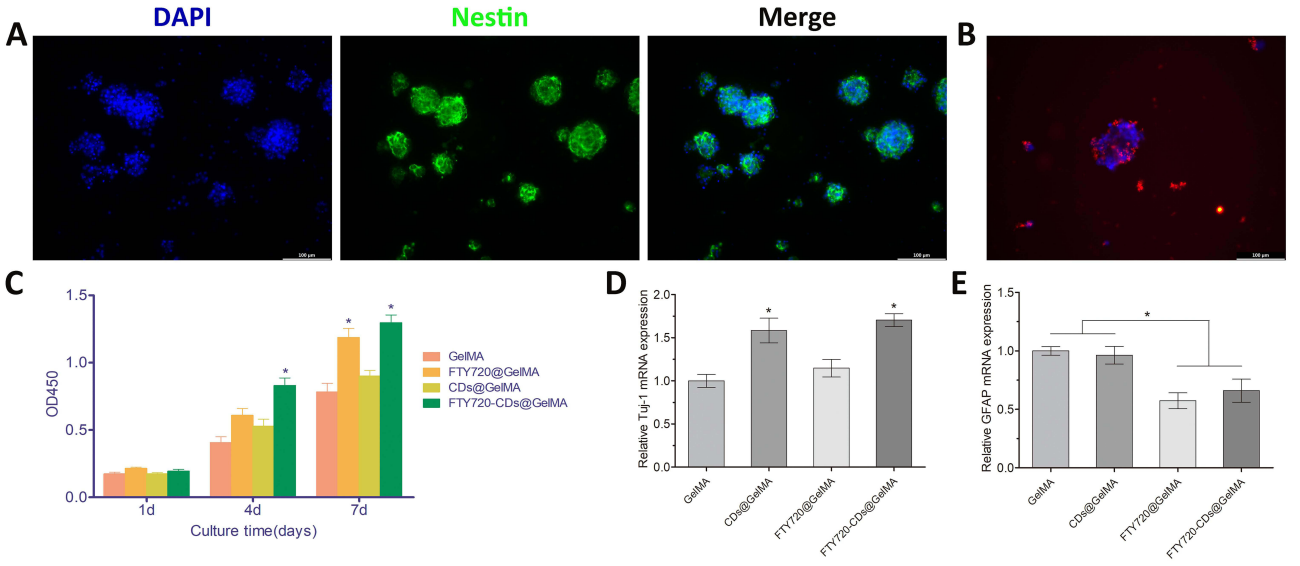

Figure 7 Proliferation of NSCs in different hydrogels. (**A**) Identification of isolated cells, which were spherical in shape and positively expressed Nestin (green). Cell nuclei were stained with DAPI (blue). Scale bar: 100 μm; (**B**) Normal growth of neural stem cells in hydrogels. Cell nuclei were stained with DAPI (blue) and neurons were stained with Tuj-1 (red), scale bar: 100 μm; (**C**) Absorbance measurements of different groups of hydrogels; (**D**) Expression of newborn neurons in different groups of hydrogels; (**E**) Expression of astrocytes in different groups of hydrogels. *Indicates P<0.05.

that the neural stem cells could grow normally in each group of hydrogels. Cell survival and proliferation in the FTY720 @GelMA and FTY720-CDs@GelMA groups were consistently maintained at a greater level from the fourth day onward, demonstrating that FTY720 has a considerable promotion effect on NSC proliferation (Figure 7C).

The restoration of spinal cord function is primarily dependent on neuronal regeneration. As a result, the number of neurons that differentiate neural stem cells after spinal cord injury is especially essential. We detected neural stem cell differentiation in different hydrogel groups using immunofluorescence (Figure 8A), and Figure 8B showed that the

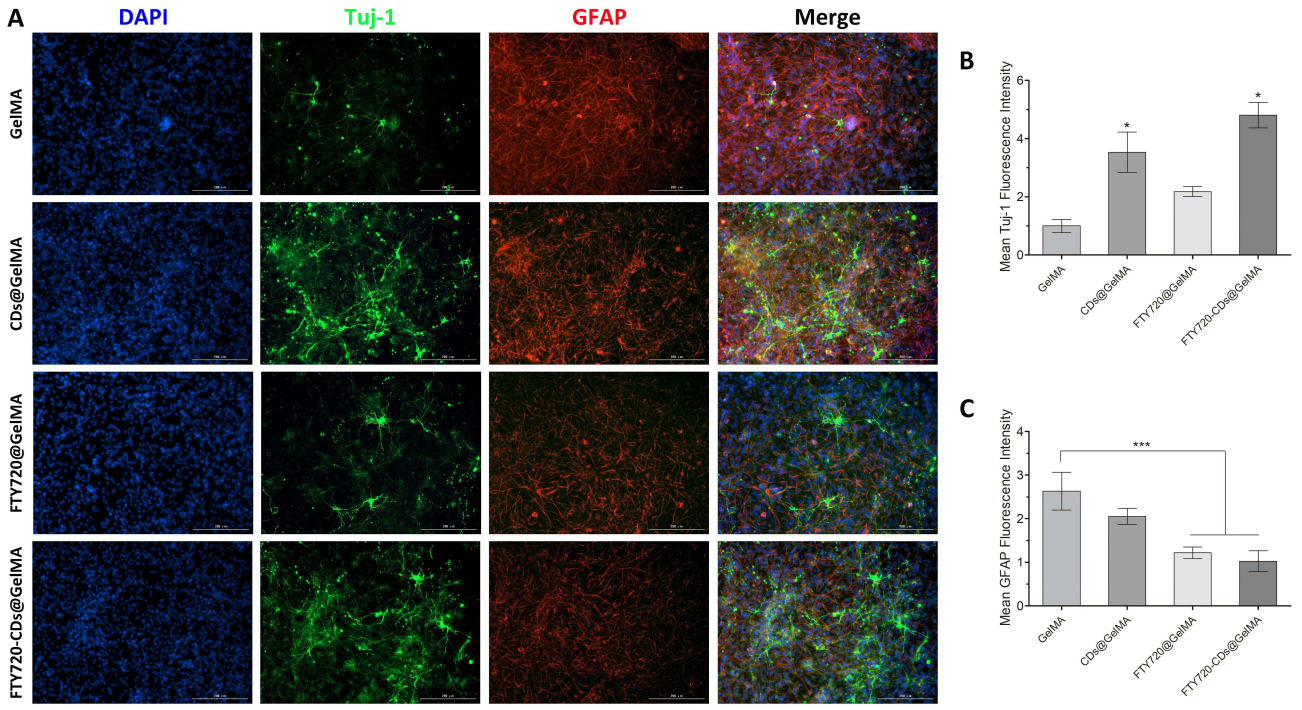

Figure 8 Regeneration of neurons at the lesion site in different groups. (**A**) Staining of newborn neurons and astrocyte staining and their fusion plots in different groups of hydrogels. Cell nuclei were stained with DAPI (blue), newborn neurons were stained with Tuj-1 (red), and astrocytes were stained with GFAP (red). Scale bar: 200 μm. (**B**) quantitative expression of newborn neurons (Tuj-1). (**C**) quantitative expression of astrocytes (GFAP). *, *** are P<0.05 and P<0.001, respectively.

neuron-ward differentiation of NSCs in the FTY720-CDs@GelMA group and the CDs@GelMA group was significantly higher than in the other groups, confirming that the addition of CDs had a significant promotion effect on the neuron-ward differentiation of NSCs. Figure 8C shows that the expression of astrocytes was dramatically reduced in the FTY720 @GelMA and FTY720-CDs@GelMA groups, showing that the addition of FTY720 could effectively restrict the differentiation of NSCs toward astrocytes. The aforesaid findings thoroughly revealed that the combination of FTY720 and CDs could successfully boost NSC proliferation and differentiation while decreasing NSC differentiation to astrocytes and better promoting SCI healing.

The differentiation of neural stem cells in different hydrogel groups was evaluated using qRT-PCR. The findings revealed that CDs@GelMA and FTY720-CDs@GelMA hydrogels facilitated NSC development into neurons (Figure 7D). Tuj-1 expression was higher in the FTY720-CDs@GelMA group than the CDs@GelMA group. We also discovered that FTY720 dramatically reduced the expression of GFAP during neural stem cell differentiation (Figure 7E). The expression of GFAP was significantly lower in the FTY720@GelMA and FTY720-CDs@GelMA groups compared to the GelMA and CDs@GelMA groups. The biological investigations showed that neural stem cells could develop in FTY720-CDs@GelMA hydrogel and differentiate into neural cells, which would aid in the functional healing of spinal cord injuries.

Functional Recovery After Spinal Cord Injury

The BBB score was used to assess motor function recovery following spinal cord damage in rats. The findings revealed that the motor function of rats in each group recovered faster after 4 weeks of injury and was essentially unchanged from 5 to 8 weeks. As demonstrated in Figure 9, the GelMA group's BBB score was much lower than the other groups, scoring only 2 points after 8 weeks. The FTY720 @GelMA group and the CDs@GelMA group had slightly higher scores than the GelMA group. After 8 weeks, the BBB scores of the FTY720-CDs@GelMA group and the FTY720-CDs+NSCs group (7.5 and 8 points, respectively) were considerably higher than those of the control group, showing that the FTY720-CDs+NSCs group may significantly increase motor function recovery after spinal cord injury.

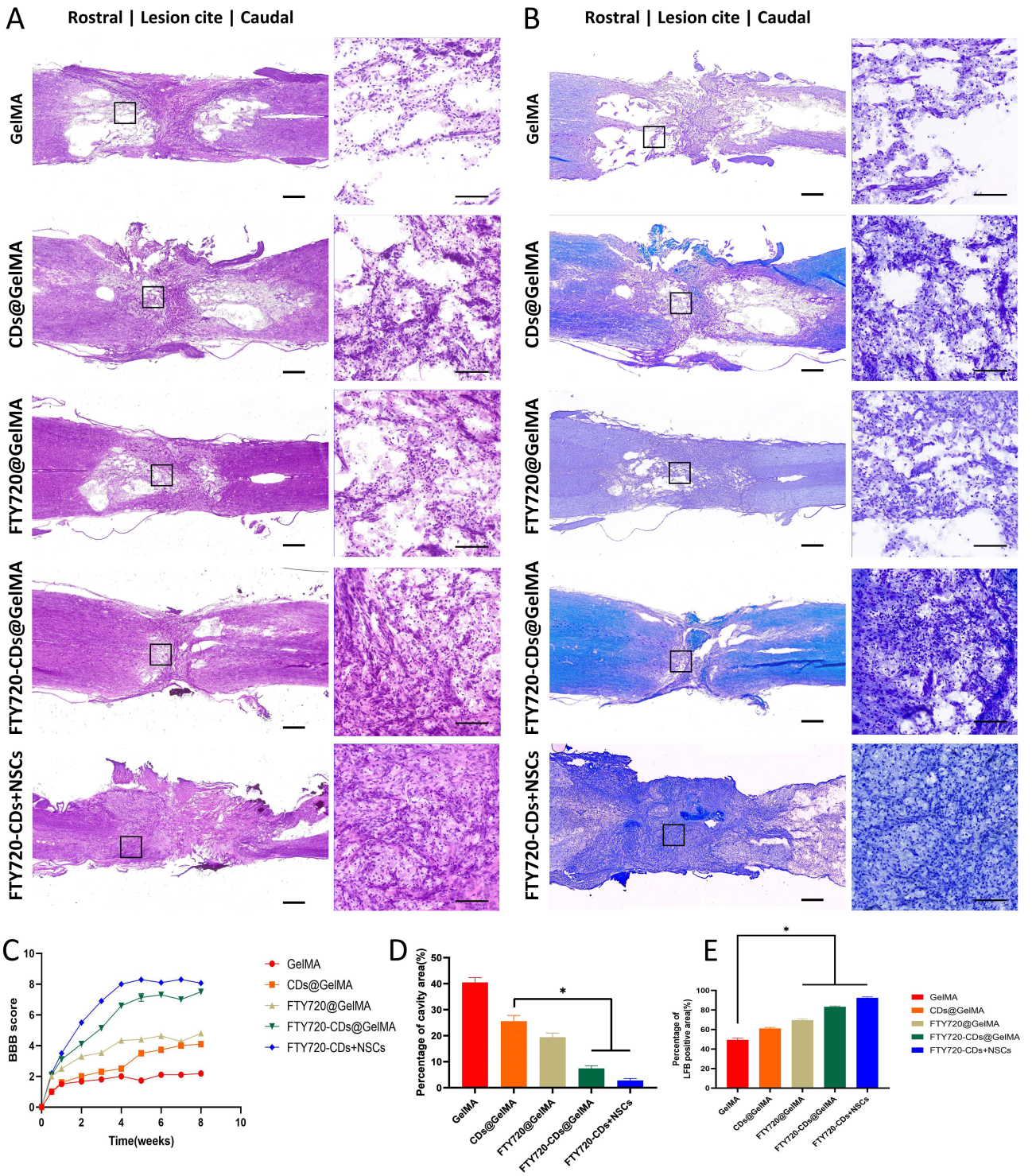

Figure 9 Evaluation of motor function recovery and tissue repair in rats 8 weeks after spinal cord injury. (**A**) HE staining of rat spinal cord in each group. Left: scale bar: 500 μm; right: scale bar: 100 μm. (**B**) LFB staining of the spinal cord of each group. The image on the right is a magnified image of the area shown in the black square on the left. Left: scale bar: 500 μm; right: scale bar: 100 μm. (**C**) BBB scores of different groups at 8 weeks post-injury. (**D**) Percentage of cavity area in each group. (**E**) Percentage of LFB-positive area in each group. *Indicates P<0.05.

Functional Recovery and Spinal Cord Regeneration After Spinal Cord Injury

After a spinal cord injury, the major pathologic alterations in the spinal cord are cystic cavities and nerve demyelination in the injury location. HE and LFB staining were utilized to assess the regeneration of spinal cord tissue following spinal cord damage. Figure 9A demonstrates that the GelMA group had a large number of cavities in the damage area, whereas

the CDs@GelMA group had fewer cavities, though the cavities were still visible. The cavity in the FTY720@GelMA group was much less than in the CDs@GelMA group. The cavity area in the FTY720-CDs@GelMA group was even less than in the FTY720@GelMA group. The FTY720-CDs+NSCs group had the best healing of the wounded area, and the injured area was almost devoid of cavity structure.

LFB staining was used to measure myelin regeneration in the affected area following spinal cord injury (Figure 9B). In the GelMA, CDs@GelMA, and FTY720@GelMA groups, myelin regeneration in the injured center was inadequate, and the LFB-positive area was 50.5%, 38.9%, and 30.3%, respectively. The proportion of LFB-positive region in the FTY720-CDs@GelMA group was significantly greater than in the first two groups (83.4%), with the FTY720-CDs +NSCs group having the highest myelin regeneration (92.5%), which was significantly higher than in the other groups (Figure 9E). The LFB-stained region was considerably greater in the FTY720@GelMA, FTY720-CDs@GelMA, and FTY720-CDs+NSCs groups compared to the control group (Figure 9E). The LFB results revealed that the combination of FTY720-CDs@GelMA and NSCs had a clear promoting effect on cavity reduction and myelin repair in the injured area. It is proposed that FTY720-CDs+NSCs can successfully enhance neural stem cell growth and differentiation in hydrogel and synapse formation, and then effectively fill the local deficiency area.

Modulation of Neurons and Astrocytes by Different Groups of Hydrogels After Spinal Cord Injury

To further validate the effect of FTY720-CDs@GelMA, a novel injectable hydrogel, on functional recovery after spinal cord damage, we used immunofluorescence labeling to detect and assess the regeneration of newborn neurons and axons in the wounded area. As demonstrated in Figure 10A, there were essentially no Tuj-1 positive cells in the GelMA group. The CDs@GelMA group had more newborn neurons than the GelMA group. Meanwhile, the number of neurons in the FTY720@GelMA group was higher than in the CDs@GelMA group, and we speculated that this was because FTY720 promoted the proliferation of local neural stem cells, which facilitated the number of differentiations toward neurons. Some neurons in the FTY720-CDs@GelMA group exhibited synaptic structures, and the number of neurons was much higher than in the GelMA, CDs@GelMA, and FTY720@GelMA groups. The FTY720-CDs+NSCs group contained the most Tuj-1-positive neurons, as well as the longest and most synapses (Figure 10C).

GFAP labeling of astrocytes. As shown in Figure 10B, GFAP staining revealed that there was a significant amount of GFAP expression in the GelMA group, as well as some GFAP expression in the CDs@GelMA group, which we hypothesized was due to CDs' excellent reactive oxygen species scavenging effect, which greatly reduced the reactive oxygen species localized to the injury and thus created a microenvironment more suitable for neural stem cell proliferation, which increased the number of neu Meanwhile, some GFAP was expressed in the FTY720@GelMA group, although it was significantly lower than in the GelMA and CDs@GelMA groups. The FTY720-CDs@GelMA group had a much lower percentage of GFAP-positive area than the other three groups. While the GFAP-positive area in the FTY720-CDs+NSCs group was greater than in the FTY720-CDs@GelMA group (Figure 10D), we hypothesized that the addition of NSCs increased local cellular accumulation and local metabolism, which resulted in an increase in astrocyte production.

Discussions

Facilitating nerve signalling in spinal cord injury recovery is a well-known international challenge.[35–37] Following spinal cord injury, there is a notable decrease in the quantity of neurons in the affected region, along with the stripping of myelin from axons and dendrites. This process interferes with the initial neuronal communication routes, resulting in impaired motor and sensory functions below the site of injury.[38,39] After an injury, the body starts the process of increasing and transforming its own neural stem cells in the damaged area to facilitate repair.[35,40,41] The impact of natural healing is restricted by adverse conditions like inflammation and oxidative stress in the injured area. Additionally, the repair process is hindered by the presence of a significant cavity at the lesion site caused by spinal cord injury.[42–44] Endogenous neural stem cells can be stimulated to migrate and differentiate following spinal cord damage, but their production rate is usually insufficient to meet the demand.[45]

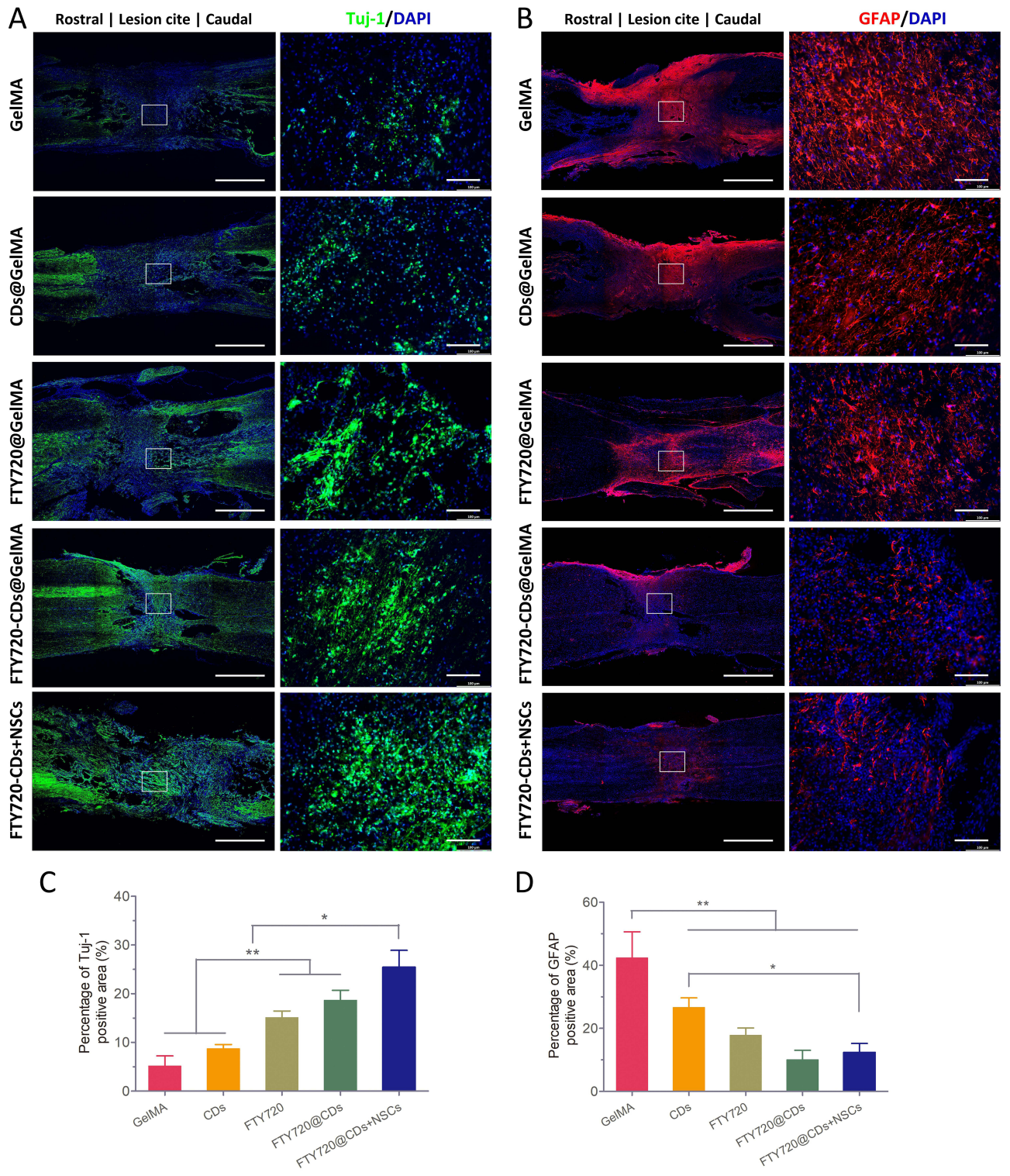

Figure 10 (**A**) Regeneration of neurons at the lesion site in different groups. Scale bar: 100 μm. (**B**) nerve fiber regeneration and axonal myelin re-formation in different groups. Scale bar: 100μm. (**C**) Percentage of Tuj-1 positive area in different groups. (**D**) Percentage of GFAP positive area in different groups. *, **P<0.05 and P<0.01, respectively.

Furthermore, the reparative effect of endogenous neural stem cells on motor function recovery following spinal cord damage has been demonstrated to be ineffective.[46] As a result, selecting appropriate biomaterials loaded with neural stem cells, medicines, or nanoparticles has promising outcomes in the treatment of spinal cord injury.[35,47,48] Because hydrogel has strong biocompatibility and breakdown ability, it was used as a carrier in this investigation to fill the damage localization in situ

for improved nutrition and supportive protection. FTY720, an FDA-approved immunosuppressant for the treatment of multiple sclerosis, has a significant protective effect on the central nervous system, and it has been demonstrated that FTY720 can significantly promote the proliferation of endogenous neural stem cells after spinal cord injury while decreasing neural stem cell differentiation to astrocytes.[49] The presence of substantial levels of local reactive oxygen species following spinal cord damage significantly impedes the repair process. As a result, identifying a biomaterial or nanoparticle capable of effectively reducing reactive oxygen species is critical.[50,51] Carbon dots (CDs) are both biocompatible and effective at scavenging reactive oxygen species. Se-CDs have comparable biocompatibility and more stable chemical characteristics, implying that they are less biotoxic and more suited for the treatment of neurological lesions.[52–54]

This work developed an injectable hydrogel containing CDs and FTY720 coupled with neural stem cells for treating spinal cord damage. All hydrogels demonstrated good biocompatibility with no internal toxicity or pathological changes after implantation. There was no accumulation of Se-CDs in any organs, indicating that the FTY720-CDs@GelMA group is safe for human application.

Following spinal cord injury (SCI), a local oxidative stress response occurred. The animal experiments showed that reactive oxygen species (ROS) results were in line with in vitro fluorescence intensity detection results. This further confirmed that FTY720-CDs@GelMA could notably decrease the inflammatory response in the SCI region, and enhance the regeneration of neurons and functional recovery post-SCI. The results suggest that FTY720-CDs@GelMA can suppress the local inflammatory response following spinal cord injury, enhance the development of new neurons and the restoration of synaptic myelin, and facilitate the improvement of motor function post-spinal cord injury. The FTY720-CDs@GelMA group demonstrated a notable advantage in scavenging reactive oxygen species. The HE staining results of the local implantation did not reveal CD accumulation. Compared to the control group, the subcutaneous implantation sites of each group exhibited minimal inflammatory reactions and inflammatory cell aggregation, confirming that the introduction of CDs does not induce local inflammation and demonstrates good biocompatibility for effective in vivo application. In the following test for reactive oxygen species (ROS) scavenging ability, it was observed that the inclusion of CDs notably improved the hydrogel's ability to scavenge ROS. The FTY720-CDs@GelMA group exhibited the highest scavenging ability for ROS, laying a solid foundation for the future use of CDs in treating localised spinal cord injuries by scavenging ROS in the affected area.

We then introduced neural stem cells into several hydrogels (Figure 7) and examined the optimal milieu for their proliferation using the CCK-8 technique and immunofluorescence. The experimental findings indicated that NSCs cells could survive in all hydrogel groups. NSCs in the FTY720-CDs@GelMA group exhibited the highest survival rate. This may be attributed to the rough surface provided by Se-CDs, which promotes NSCs adhesion and growth. Additionally, the introduction of FTY720 significantly boosts NSCs proliferation and enhances cell survival. We discovered that CDs@GelMA and FTY720-CDs@GelMA hydrogels enhanced the differentiation of NSCs into neurons. Tuj-1 expression increased in the FTY720-CDs@GelMA group compared to the CDs@GelMA group. Additionally, we discovered that the injection of FTY720 notably decreased the expression of GFAP while neural stem cells were differentiating. The GFAP expression level was significantly lower in the FTY720@GelMA and FTY720-CDs@GelMA groups compared to the GelMA and CDs@GelMA groups. These results align with CDs promoting neuronal differentiation of NSCs, FTY720 inhibiting NSCs, and CDs inhibiting NSCs as well as FTY720 inhibiting NSCs differentiation into astrocytes.

Immunofluorescence findings indicated that the combination of FTY720-CDs@GelMA enhanced both the quantity and size of neuronal synapses, resulting in stronger synaptic connections between neurons. The formation of new neurons and myelin sheaths is crucial for the restoration of nerve function. The number of neurons in the FTY720@GelMA group was higher than in the CDs@GelMA group. This increase may be attributed to the larger number of neural stem cells (NSCs) under the influence of FTY720, leading to a greater number of cells without promoting differentiation. The ratio of trends remains constant as the number of NSCs rises. The study demonstrated a rise in the number of neural stem cells (NSCs), leading to a corresponding increase in NSC differentiation. Neurons in the FTY720-CDs@GelMA group showed synaptic structures and a considerably higher number compared to the GelMA, CDs@GelMA, and FTY720@GelMA groups. The group treated with FTY720-CDs+NSCs had the highest quantity of Tuj-1-positive neurons, as well as substantially longer and more numerous synapses compared to the other groups. Astrocytes have the ability to release collagen, which hinders the restoration of neuronal function. Our investigation discovered that FTY720-CDs@GelMA notably decreased the quantity of astrocytes. The double immunostaining results in Figure 8 showed that CDs promoted the conversion of endogenous NSCs into new neurons.

Additionally, FTY720 was found to decrease the transformation of NSCs into astrocytes. The combination of FTY720 with Se-CDs synergistically enhanced the differentiation of NSCs into neurons (Tuj-1) and reduced the differentiation of NSCs into astrocytes (GFAP). The cellular experimental results above confirmed that FTY720-CDs@GelMA can enhance the proliferation and differentiation of neural stem cells into neurons, increase the quantity and length of cellular synapses, enhance the regeneration of myelin sheaths, and aid in the reconstruction of nerve function.

Motor recovery was evaluated using the Basso, Beattie, and Bresnahan (BBB) score 8 weeks post-injury. The study results indicated that there was no notable distinction between the CDs@GelMA group and the FTY720@GelMA group. The FTY720-CDs@GelMA group achieved a score of 8 after 8 weeks, the highest among all groups, demonstrating that FTY720-CDs@GelMA effectively enhances motor function recovery after SCI. Cystic cavities of varying diameters develop in the location of the spinal cord damage. The presence of these holes hinders the regeneration of the spinal cord. Through HE staining and LFB staining (Figure 9), it was seen that FTY720-CDs@GelMA effectively decreased the size of the cavity in the injured area. Additionally, FTY720-CDs@GelMA enhanced the recovery of the damaged region, suggesting increased cell production in that location. LFB is a staining agent used to specifically target myelin proteins, the primary constituents of axons and the predominant elements of myelin. Myelin regeneration was most pronounced in the FTY720-CDs+NSCs group, surpassing all other groups significantly. The results indicate that introducing NSCs and using FTY720 and CDs together can greatly enhance the proliferation of local neural stem cells in spinal cord injury. Additionally, this combination significantly boosts the neuronal differentiation of NSCs, leading to increased formation of myelin sheaths in the affected area. These findings align with the outcomes of in vitro cellular studies.

Spinal cord injury repair necessitates neuronal regeneration, which was evaluated using immunofluorescence labelling to determine the quantity of regenerated neurons (Figure 10). We observed a considerable increase in the number of new neurons in the FTY720-CDs@GelMA group. The results indicate that the combination of FTY720 and CDs in FTY720-CDs@GelMA successfully enhanced the proliferation and differentiation of endogenous neural stem cells into new neurons following spinal cord injury. Following neuronal regeneration, the focus shifts to establishing inter-neuronal signalling pathways, mostly through the development of axons and synapses. GFAP staining results indicated minimal positive expression in the injury centre in both the FTY720-CDs@GelMA group and the FTY720-CDs+NSCs group. The remaining groups could discover a significant level of positive expression in the harm centre. The GFAP-positive area was increased in the FTY720-CDs+NSCs group compared to the FTY720-CDs@GelMA group. This increase may be attributed to the introduction of NSCs, which potentially elevated the number of NSCs in the local area, consequently enhancing local cellular metabolism and astrocyte production. The results indicate that the simultaneous use of FTY720-CDs + NSCs can greatly enhance neurite development and reduce astrocyte production, promoting the restoration of brain signalling networks.[55–57]

The experimental findings demonstrated that Se-CDs could be securely attached within the internal framework of GelMA. Additionally, Se-CDs enhanced the hydrogel's anti-inflammatory and antioxidant capabilities, aligning with their function in other biomaterials. FTY720 introduction could decrease astrocyte synthesis and enhance neuron regeneration and axon growth following spinal cord injury, thereby aiding in spinal cord injury recovery.

Conclusion

In this study, we created an injectable composite hydrogel FTY720-CDs@GelMA loaded with CDs and FTY720 and paired it with NSCs for the therapy of SCI. This new hydrogel is biocompatible. The CDs enhanced the hydrogel's ROS scavenging ability, antioxidant impact, and encouragement of neuronal differentiation of NSCs. FTY720 stimulated the growth of damaged neural stem cells while inhibiting their maturation into astrocytes. In vitro tests revealed that FTY720-CDs @GelMA hydrogel increased NSC proliferation and differentiation to create neonatal neurons while decreasing NSC differentiation to astrocytes. In vivo experiments revealed that this novel treatment of FTY720-CDs@GelMA hydrogel in combination with NSCs significantly reduced the area of the injury cavity and demyelination changes, promoted the formation of new neurons and synapses in the area of the injury, and reduced the formation of glial scars in the area of the injury. Furthermore, it dramatically increased the recovery of motor function in rats following spinal cord injury, presenting a novel strategy to the treatment of spinal cord injury.

Ethics Approval and Consent

The use of experimental animals in this study has been approved by the Institutional Animal Care and Use Committee of Jilin University. All procedures strictly adhere to the guidelines for the care and utilization of experimental animals set forth by Jilin University.

Funding

This work was supported by the National Natural Science Foundation of China (82002301, 82171388) and Bethune Project of Jilin University (2022B43).

Disclosure

The authors report no conflicts of interest in this work.

References

1. Faulkner JR, Herrmann JE, Woo MJ, Tansey KE, Doan NB, Sofroniew MV. Reactive astrocytes protect tissue and preserve function after spinal cord injury. *J Neurosci*. 2004;24(9):2143–2155. doi:10.1523/jneurosci.3547-03.2004
2. David S, Kroner A. Repertoire of microglial and macrophage responses after spinal cord injury. *Nat Rev Neurosci*. 2011;12(7):388–399. doi:10.1038/nrn3053
3. Huang WL, George KJ, Ibba V, et al. The characteristics of neuronal injury in a static compression model of spinal cord injury in adult rats. *Eur J Neurosci*. 2007;25(2):362–372. doi:10.1111/j.1460-9568.2006.05284.x
4. Sofroniew MV. Dissecting spinal cord regeneration. *Nature*. 2018;557(7705):343–350. doi:10.1038/s41586-018-0068-4
5. Fan BY, Wei ZJ, Yao X, et al. Microenvironment imbalance of spinal cord injury. *Cell Transpl*. 2018;27(6):853–866. doi:10.1177/0963689718755778
6. Song YH, Agrawal NK, Griffin JM, Schmidt CE. Recent advances in nanotherapeutic strategies for spinal cord injury repair. Review. *Adv Drug Delivery Rev*. 2019;148:38–59. doi:10.1016/j.addr.2018.12.011
7. Amanda Phuong T, Warren PM, Silver J. The biology of regeneration failure and success after spinal cord injury. Review. *Physiol Rev*. 2018;98 (2):881–917. doi:10.1152/physrev.00017.2017
8. Zhou XH, Shi GD, Fan BY, et al. Polycaprolactone electrospun fiber scaffold loaded with iPSCs-NSCs and ASCs as a novel tissue engineering scaffold for the treatment of spinal cord injury. *Int J Nanomed*. 2018;13:6265–6277. doi:10.2147/ijn.S175914
9. Rao YJ, Zhu WX, Guo YX, et al. Long-term outcome of olfactory ensheathing cell transplantation in six patients with chronic complete spinal cord injury. *Cell Transpl*. 2013;22:S21–S25. doi:10.3727/096368913x672127
10. Barnabe-Heider F, Frisen J. Stem cells for spinal cord repair. *Cell Stem Cell*. 2008;3(1):16–24. doi:10.1016/j.stem.2008.06.011
11. Yin W, Li X, Zhao YN, et al. Taxol-modified collagen scaffold implantation promotes functional recovery after long-distance spinal cord complete transection in canines. *Biomater Sci*. 2018;6(5):1099–1108. doi:10.1039/c8bm00125a
12. Li X, Zhao YN, Cheng SX, et al. Cetuximab modified collagen scaffold directs neurogenesis of injury-activated endogenous neural stem cells for acute spinal cord injury repair. *Biomaterials*. 2017;137:73–86. doi:10.1016/j.biomaterials.2017.05.027
13. Chen C, Zhao ML, Zhang RK, et al. Collagen/heparin sulfate scaffolds fabricated by a 3D bioprinter improved mechanical properties and neurological function after spinal cord injury in rats. *J Biomed Mater Res Part A*. 2017;105(5):1324–1332. doi:10.1002/jbm.a.36011
14. Geissler SA, Sabin AL, Besser RR, et al. Biomimetic hydrogels direct spinal progenitor cell differentiation and promote functional recovery after spinal cord injury. *J Neural Eng*. 2018;15(2):025004. doi:10.1088/1741-2552/aaa55c
15. Liu K, Dong XZ, Wang Y, Wu XP, Dai HL. Dopamine-modified chitosan hydrogel for spinal cord injury. *Carbohydr Polym*. 2022;2022:298120047. doi:10.1016/j.carbpol.2022.120047
16. Xu C, Chang YK, Wu P, et al. Two-dimensional-germanium phosphide-reinforced conductive and biodegradable hydrogel scaffolds enhance spinal cord injury repair. *Adv Funct Mater*. 2021;31(41):2104440. doi:10.1002/adfm.202104440
17. Long YP, Yan LS, Dai HL, et al. Enhanced proliferation and differentiation of neural stem cells by peptide-containing temperature-sensitive hydrogel scaffold. *Mater Sci Eng C Mater Biol Appl*. 2020:116111258. doi:10.1016/j.msec.2020.111258
18. Fuhrmann T, Anandakumaran PN, Shoichet MS. Combinatorial therapies after spinal cord injury: how can biomaterials help? *Adv Healthcare Mater*. 2017;6(10):1601130. doi:10.1002/adhm.201601130
19. Hu SQ, Zhou L, Tu LJ, et al. Elastomeric conductive hybrid hydrogels with continuous conductive networks. *J Mat Chem B*. 2019;7 (15):2389–2397. doi:10.1039/c9tb00173e
20. Jiang YQ, Fu PF, Liu YY, et al. Near-infrared light-triggered NO release for spinal cord injury repair. *Sci Adv*. 2020;6(39):eabc3513. doi:10.1126/sciadv.abc3513
21. Anwar MA, Al Shehabi TS, Eid AH. Inflammogenesis of secondary spinal cord injury. *Front Cell Neurosci*. 2016;1098. doi:10.3389/fncel.2016.00098
22. Azbill RD, Mu X, Bruce-Keller AJ, Mattson MP, Springer JE. Impaired mitochondrial function, oxidative stress and altered antioxidant enzyme activities following traumatic spinal cord injury. *Brain Res*. 1997;765(2):283–290. doi:10.1016/s0006-8993(97)00573-8
23. Kullmann AF, Truschel ST, Wolf-Johnston AS, et al. Acute spinal cord injury is associated with mitochondrial dysfunction in mouse urothelium. *Neurourol Urodynamics*. 2019;38(6):1551–1559. doi:10.1002/nau.24037
24. Zhang T, Lin F, Liu W, et al. Reactive oxide species-scavenging lipid-polymer nanoparticles for neuroprotection after spinal cord injury. Article. *Appl Mater Today*. 2021:24101109. doi:10.1016/j.apmt.2021.101109
25. Chen X, Cui J, Zhai X, et al. Inhalation of hydrogen of different concentrations ameliorates spinal cord injury in mice by protecting spinal cord neurons from apoptosis, oxidative injury and mitochondrial structure damages. Article. *Cell Physiol Biochem*. 2018;47(1):176–190. doi:10.1159/000489764

26. Ji Z, Zheng J, Ma Y, et al. Emergency treatment and photoacoustic assessment of spinal cord injury using reversible dual-signal transform-based selenium antioxidant. Article; Early Access. *Small*. 2023. doi:10.1002/smll.202207888
27. Li F, Li T, Sun C, Xia J, Jiao Y, Xu H. Selenium-doped carbon quantum dots for free-radical scavenging. Article. *Angew Chem*. 2017;56 (33):9910–9914. doi:10.1002/anie.201705989
28. Luo W, Wang Y, Lin F, et al. Selenium-doped carbon quantum dots efficiently ameliorate secondary spinal cord injury via scavenging reactive oxygen species. Article. *Int J Nanomed*. 2020;15:10113–10125. doi:10.2147/ijn.S282985
29. Huang G, Lin Y, Zhang L, Yan Z, Wang Y, Liu Y. Synthesis of sulfur-selenium doped carbon quantum dots for biological imaging and scavenging reactive oxygen species. Article. *Sci Rep*. 2019;919651. doi:10.1038/s41598-019-55996-w
30. Teng YD, Lavik EB, Qu XL, et al. Functional recovery following traumatic spinal cord injury mediated by a unique polymer scaffold seeded with neural stem cells. *Proc Natl Acad Sci USA*. 2002;99(5):3024–3029. doi:10.1073/pnas.052678899
31. Puga DA, Toyar CA, Guan Z, et al. Stress exacerbates neuron loss and microglia proliferation in a rat model of excitotoxic lower motor neuron injury. *Brain Behav Immun*. 2015;49:246–254. doi:10.1016/j.bbi.2015.06.006
32. Lee KD, Chow WN, Sato-Bigbee C, et al. FTY720 reduces inflammation and promotes functional recovery after spinal cord injury. *J Neurotrauma*. 2009;26(12):2335–2344. doi:10.1089/neu.2008.0840
33. Li Y, Chen Y, Hu X, et al. Fingolimod (FTY720) hinders interferon-gamma-mediated fibrotic scar formation and facilitates neurological recovery after spinal cord injury. Article; Early Access. *J Neurotrauma*. 2023. doi:10.1089/neu.2022.0387
34. Yamazaki K, Kawabori M, Seki T, et al. FTY720 attenuates neuropathic pain after spinal cord injury by decreasing systemic and local inflammation in a rat spinal cord compression model. Article. *J Neurotrauma*. 2020;37(15):1720–1728. doi:10.1089/neu.2019.6905
35. Xu Y, Zhou J, Liu C, et al. Understanding the role of tissue-specific decellularized spinal cord matrix hydrogel for neural stem/progenitor cell microenvironment reconstruction and spinal cord injury. Article. *Biomaterials*. 2021:268120596. doi:10.1016/j.biomaterials.2020.120596
36. Leibinger M, Zeitler C, Gobrecht P, Andreadaki A, Gisselmann G, Fischer D. Transneuronal delivery of hyper-interleukin-6 enables functional recovery after severe spinal cord injury in mice. Article. *Nat Commun*. 2021;12(1):391. doi:10.1038/s41467-020-20112-4
37. Wang Y, Lai X, Wu D, Liu B, Wang N, Rong L. Umbilical mesenchymal stem cell-derived exosomes facilitate spinal cord functional recovery through the miR-199a-3p/145-5p-mediated NGF/TrkA signaling pathway in rats. Article. *Stem Cell Res Ther*. 2021;12(1):117. doi:10.1186/s13287-021-02148-5
38. Khodabandeh Z, Mehrabani D, Dehghani F, et al. Spinal cord injury repair using mesenchymal stem cells derived from bone marrow in mice: a stereological study. Article. *Acta Histochem*. 2021;123(5):151720. doi:10.1016/j.acthis.2021.151720
39. Noori L, Arabzadeh S, Mohamadi Y, et al. Intrathecal administration of the extracellular vesicles derived from human Wharton's jelly stem cells inhibit inflammation and attenuate the activity of inflammasome complexes after spinal cord injury in rats. Article. *Neurosci Res*. 2021;170:87–98. doi:10.1016/j.neures.2020.07.011
40. Yuan T, Shao Y, Zhou X, et al. Highly permeable DNA supramolecular hydrogel promotes neurogenesis and functional recovery after completely transected spinal cord injury. Article. *Adv Mater*. 2021;33(35):2102428. doi:10.1002/adma.202102428
41. Yang Y, Fan Y, Zhang H, et al. Small molecules combined with collagen hydrogel direct neurogenesis and migration of neural stem cells after spinal cord injury. Article. *Biomaterials*. 2021:269120479. doi:10.1016/j.biomaterials.2020.120479
42. Yang B, Liang C, Chen D, et al. A conductive supramolecular hydrogel creates ideal endogenous niches to promote spinal cord injury repair. Article. *Bioact Mater*. 2022;15:103–119. doi:10.1016/j.bioactmat.2021.11.032
43. Zhou K, Chen H, Xu H, Jia X. Trehalose augments neuron survival and improves recovery from spinal cord injury via mTOR-independent activation of autophagy. Article. *Oxid Med Cell Longev*. 2021;20218898996. doi:10.1155/2021/8898996
44. Li Y, Qiu H, Yao S, et al. Geniposide exerts protective effects on spinal cord injury in rats by inhibiting the IKKs/NF-kappa B signaling pathway. Article. *Int Immunopharmacol*. 2021:100108158. doi:10.1016/j.intimp.2021.108158
45. Lindvall O, Kokaia Z. Stem cells in human neurodegenerative disorders - time for clinical translation? *J Clin Investig*. 2010;120(1):29–40. doi:10.1172/jci40543
46. Katoh H, Yokota K, Fehlings MG. Regeneration of spinal cord connectivity through stem cell transplantation and biomaterial scaffolds. *Front Cell Neurosci*. 2019;13248. doi:10.3389/fncel.2019.00248
47. Shen H, Xu B, Yang C, et al. A DAMP-scavenging, IL-10-releasing hydrogel promotes neural regeneration and motor function recovery after spinal cord injury. *Biomaterials*. 2022:280121279. doi:10.1016/j.biomaterials.2021.121279
48. Fan L, Liu C, Chen XX, et al. Exosomes-loaded electroconductive hydrogel synergistically promotes tissue repair after spinal cord injury via immunoregulation and enhancement of myelinated axon growth. *Adv Sci*. 2022;9(13):2105586. doi:10.1002/advs.202105586
49. Kimura A, Ohmori T, Ohkawa R, et al. Essential roles of sphingosine 1-phosphate/$S1P_1$ receptor axis in the migration of neural stem cells toward a site of spinal cord injury. *Stem Cells*. 2007;25(1):115–124. doi:10.1634/stemcells.2006-0223
50. Liu ZY, Yao XQ, Sun BH, et al. Pretreatment with kaempferol attenuates microglia-mediate neuroinflammation by inhibiting MAPKs–NF–κB signaling pathway and pyroptosis after secondary spinal cord injury. *Free Radic Biol Med*. 2021;168:142–154. doi:10.1016/j.freeradbiomed.2021.03.037
51. Ge MH, Tian H, Mao L, et al. Zinc attenuates ferroptosis and promotes functional recovery in contusion spinal cord injury by activating Nrf2/GPX4 defense pathway. *CNS Neurosci Ther*. 2021;27(9):1023–1040. doi:10.1111/cns.13657
52. Liao J, Yao Y, Lee C-H, Wu Y, Li P. In vivo biodistribution, clearance, and biocompatibility of multiple carbon dots containing nanoparticles for biomedical application. Article. *Pharmaceutics*. 2021;13(11):1872. doi:10.3390/pharmaceutics13111872
53. Sajjad F, Han Y, Bao L, et al. The improvement of biocompatibility by incorporating porphyrins into carbon dots with photodynamic effects and pH sensitivities. Article. *J Biomater Appl*. 2022;36(8):1378–1389. doi:10.1177/08853282211050449
54. Chen X, Qin Y, Song X, et al. Green synthesis of carbon dots and their integration into Nylon-11 nanofibers for enhanced mechanical strength and biocompatibility. Article. *Nanomaterials*. 2022;12(19):3347. doi:10.3390/nano12193347
55. Shao A, Tu S, Lu J, Zhang J. Crosstalk between stem cell and spinal cord injury: pathophysiology and treatment strategies. Review. *Stem Cell Res Ther*. 2019;10(1):238. doi:10.1186/s13287-019-1357-z
56. Anjum A, Yazid MD, Fauzi Daud M, et al. Spinal cord injury: pathophysiology, multimolecular interactions, and underlying recovery mechanisms. Review. *Int J Mol Sci*. 2020;21(20):7533. doi:10.3390/ijms21207533
57. Jiang D, Yang X, Ge M, et al. Zinc defends against Parthanatos and promotes functional recovery after spinal cord injury through SIRT3-mediated anti-oxidative stress and mitophagy. Article; Early Access. *CNS Neurosci Ther*. 2023. doi:10.1111/cns.14222